













Optical properties of germania and titania at 1064 nm and at 1550 nm

D Diksha^{1,2,*}, A Amato^{1,2} , V Spagnuolo^{1,2} ,
G I McGhee³ , M Chicoine⁴ , C Clark⁵, S Hill³, J Hough³ ,
R Johnston³ , R Keil¹ , N Mavridi⁵, S Reid⁶, S Rowan³ ,
T Schapals¹, F Schiettekatte⁴ , S C Tait³ , I W Martin³ ,
and J Steinlechner^{1,2,3,*} 

¹ Maastricht University, Minderbroedersberg 4-6, 6211 LK Maastricht, The Netherlands

² Nikhef, Science Park 105, 1098 XG Amsterdam, The Netherlands

³ SUPA, School of Physics and Astronomy, University of Glasgow, Glasgow G12 8QQ, United Kingdom

⁴ Département de physique, Université de Montréal, Montréal, Québec H3C 3J7, Canada

⁵ Helia Photonics, Rosebank Technology Park Unit 2, Livingston EH54 7EJ, United Kingdom

⁶ SUPA, Department of Biomedical Engineering, University of Strathclyde, Glasgow G4 ONW, United Kingdom

E-mail: d.diksha@maastrichtuniversity.nl and
jessica.steinlechner@maastrichtuniversity.nl

Received 4 January 2024; revised 20 March 2024

Accepted for publication 9 April 2024

Published 17 May 2024



CrossMark

Abstract

One of the main noise sources in current gravitational-wave detectors is the thermal noise of the high-reflectivity coatings on the main interferometer optics. Coating thermal noise is dominated by the mechanical loss of the high-refractive index material within the coating stacks, Ta_2O_5 mixed with TiO_2 . For upgrades to room-temperature detectors, a mixture of GeO_2 and TiO_2 is an interesting alternative candidate coating material. While the rather low refractive index of GeO_2 increases with increasing TiO_2 content, a higher TiO_2 content results in a lower threshold temperature before heat treatment leads to crystallisation, and potentially to a degradation of optical properties.

* Authors to whom any correspondence should be addressed.



Original Content from this work may be used under the terms of the [Creative Commons Attribution 4.0 licence](https://creativecommons.org/licenses/by/4.0/). Any further distribution of this work must maintain attribution to the author(s) and the title of the work, journal citation and DOI.

For future cryogenic detectors, on the other hand, a higher TiO₂ content is beneficial as the TiO₂ suppresses the low-temperature mechanical loss peak of GeO₂. In this paper, we present the optical properties of coatings—produced by plasma-assisted ion-beam evaporation—with high TiO₂ content at 1550 nm, a laser wavelength considered for cryogenic gravitational-wave detectors, as a function of heat-treatment temperature. For comparison, the absorption of pure GeO₂ was also measured. Furthermore, results at the currently-used wavelength of 1064 nm are presented.

Keywords: gravitational-wave detectors, coating thermal noise, titania, low temperature, absorption

1. Introduction

The first detection of gravitational waves, a transient signal produced by the merger of two stellar-mass black holes, was announced in 2016 [1]. Since then, many more signals have been detected [2, 3] by the Advanced LIGO [4] and Advanced Virgo [5] gravitational-wave detectors.

In the frequency range between ≈ 30 Hz and a few hundred Hz, thermal noise of the highly-reflective mirror coatings is one of the limiting noise sources in gravitational-wave detectors [6], preventing more signals from weaker or more distant astrophysical sources being observed. Typically, a highly-reflective coating is made of alternating layers of high- and low-refractive index materials, where the reflectivity increases with the refractive index contrast and the number of layers. The amplitude spectral density of the coating thermal noise (CTN) as a function of frequency f is proportional to the square root of the mirror temperature T , the coating thickness d , the mechanical loss ϕ , and inversely proportional to the laser beam radius on the mirror w [7]:

$$x(f) \propto \sqrt{\frac{Td}{w^2\phi}}, \quad (1)$$

assuming for simplicity that the mechanical losses associated with bulk motion and shear motion [8] are approximately equal ($\phi_{\text{bulk}} \approx \phi_{\text{shear}} \approx \phi$).

The materials used in the current Advanced LIGO and Advanced Virgo coatings are SiO₂ for the low-refractive index material and a mixture of TiO₂ and Ta₂O₅ (TiO₂:Ta₂O₅) for the high refractive index material, deposited on SiO₂ substrates [9]. In order to reduce CTN as expressed by equation (1), possible solutions include the reduction of d , by increasing the refractive index contrast while preserving the design reflectivity, and ϕ . TiO₂:Ta₂O₅ dominates CTN as it has a mechanical loss angle much higher than that of SiO₂ [9]. Therefore, finding alternative high-refractive index materials is a promising way forward for reducing CTN.

Alternative high-index material options are being explored, such as ZrO₂ [10], Nb₂O₅ [11], HfO₂ [12], SiN_x [13–15], mixtures of TiO₂ with SiO₂ [16] and many others. Recent studies have shown that the mechanical loss of amorphous thin film coatings is correlated with the atomic order [17–21]. Further investigations on heat-treatment and optimization of coating performance by understanding atomic structure and relaxation processes demonstrated that SiO₂ has a prevalence of corner-sharing structure and that this characteristic could confer good mechanical properties to the material [19, 22]. Moreover, several oxides were explored, showing that in particular GeO₂ exhibited a local atomic order similar to SiO₂ and additional post-deposition heat treatment or high temperature deposition can improve the structural organization up to the medium-range, resulting in a lower mechanical loss [18, 20, 22–25].

GeO₂ has a significantly lower refractive index ($n = 1.60$ at 1064 nm—see table 2) than TiO₂:Ta₂O₅ ($n = 2.05$ at 1064 nm [26]) making it unsuitable as a replacement for the high-index material combined with SiO₂ low-index layers, as a large number of layers would be required to achieve high reflectivity, which in turn would increase CTN. Mixing GeO₂ with TiO₂ could be a possible solution as TiO₂ has a significantly higher refractive index between 2.3 and 2.5 when produced by ion beam sputtering [27, 28], and slightly lower—between around 2.0 and 2.25 depending on the exact deposition conditions and resulting density [29]—when produced by reactive evaporation. Vajente *et al* [28] recently studied the mechanical properties of pure GeO₂ and mixtures with 27% and 44% TiO₂, finding promising low CTN for a mixture of 56% GeO₂ and 44% TiO₂ at room temperature.

As a reduction in temperature is also a way to reduce CTN, see equation (1), cryogenic operation is considered for future gravitational-wave detectors such as the Einstein Telescope [30] and LIGO Voyager [31]. GeO₂ shows a low-temperature mechanical loss peak very similar to that of SiO₂, which decreases with increasing TiO₂ content [32], making even higher TiO₂ concentrations particularly interesting for use at low temperatures. For pure TiO₂, a drop in low temperature loss after crystallisation has been observed [33]. Low-temperature operation makes SiO₂ unsuitable as a mirror substrate material for gravitational-wave detectors due to an increase in mechanical loss, and a change to crystalline silicon is considered. This in turn requires a change from 1064 nm to a laser wavelength at which silicon is transparent, e.g. 1550 nm.

In this paper, we present the optical absorption and refractive index at 1550 nm of TiO₂ with a small amount of GeO₂ mixed in during deposition and, for comparison, of pure GeO₂. For the context of the coating quality, we also present results measured at 1064 nm. We find that the optical absorption of both TiO₂ and GeO₂ is larger at 1550 nm than at 1064 nm, while at 1064 nm it is comparable to other coating materials of interest [28]. Interestingly, while the absorption of both materials initially decreases with heat treatment, the absorption of GeO₂ starts to increase above a certain temperature, while that of TiO₂ remains low, beyond the crystallisation temperature.

2. Coating deposition and composition

The coatings were deposited on SiO₂ substrates (Corning 7979 and 7980), 25.4 mm in diameter and 3 mm thick, by Helia Photonics using plasma ion-assisted electron beam evaporation.

As target materials, Ti₃O₅ (99.9% purity) and Ge (99.999% purity) were used. Targets were prepared by mixing different ratios of the two materials. Subsequently, evaporation was carried out using an electron beam in a 25 cm³ graphite liner at approximately 2 kW heating power, resulting in deposition rates of approximately 3 Å s⁻¹. During deposition, the process was reactively densified under a partial Ar/O₂ atmosphere at 1.4×10^{-4} mbar, aided by a 43 A plasma current at 140 V and quartz radiative heaters, maintaining substrates at 100 °C. A starting pressure of 2×10^{-6} mbar was standard for these depositions, with the chamber being evacuated by a diffusion pump and cryocoil.

Due to the different vapour pressures of Ti₃O₅ and Ge, for three targets with lower Ti₃O₅ content ($\leq 50\%$), i.e. Run 1, 2 and 3, the resulting coatings were almost pure GeO₂, while for a high Ti₃O₅ of $\approx 95\%$, i.e. Run 4, an almost pure TiO₂ layer was obtained. However, instead of a homogeneous mixture of the two materials, a layer structure of pure TiO₂ surrounded by thin layers containing Ge was created. The measured composition of the four coating runs produced is presented in table 1. Figure 1 shows the atomic concentration distribution for Run 1 as an example of a pure GeO₂ deposition and for the layer structure of Run 4. In order to

Table 1. Measured coating thickness and composition in atomic percentage (at. %) of the coatings as deposited from the four deposition runs. Coating Run 4 displayed a layered structure which is presented as top, middle and bottom layer with the bottom being the closest to the substrate.

| Run | Layer | thickness (nm) | O ± 3% | Ar ± 0.2% | Ge ± 0.2% | Ti ± 0.2% | Si ± 0.2% |
|-------|--------|----------------|-----------|--------------|--------------|--------------|--------------|
| Run 1 | | 533 ± 7 | 69 | 0.50 | 30.5 | 0.0 | 0.0 |
| Run 2 | | 584 ± 10 | 69 | 0.40 | 30.5 | 0.1 | 0.0 |
| Run 3 | | 459 ± 5 | 71 | 0.70 | 28.0 | 0.3 | 0.0 |
| Run 4 | top | 29.1 ± 0.3 | 66 | 0.3 | 12.0 | 21.4 | 0.0 |
| | middle | 562 ± 6 | 68 | 0.5 | 0.3 | 31.0 | 0.5 |
| | bottom | 54 ± 0.5 | 67 | 0.3 | 26.0 | 7.0 | 0.5 |

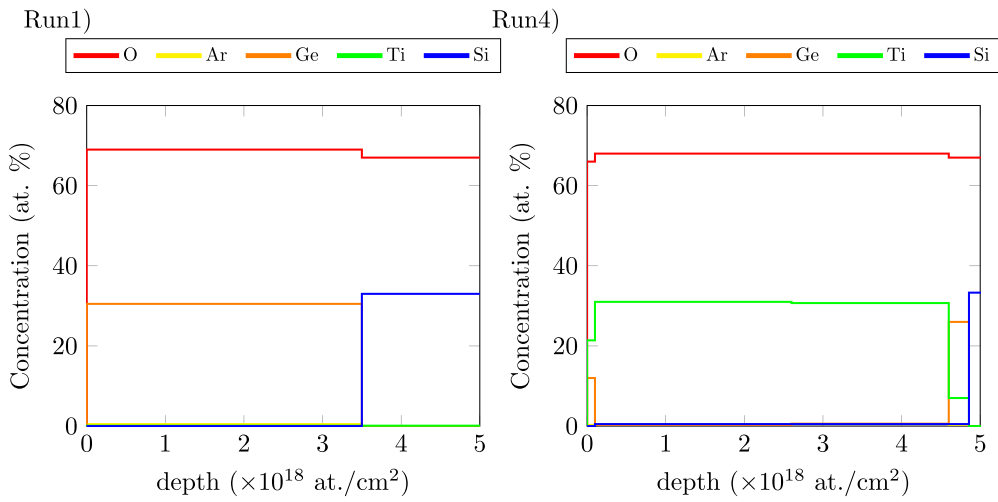


Figure 1. Atomic percentage composition of the coatings from Run 1 and 4 as deposited as function of layer depth expressed in atoms per cm^2 . The deepest layer, with larger Si atomic concentration is the silica substrate.

determine the composition of each coating of the different deposition runs, Rutherford backscattering spectrometry (RBS) [34] was carried out on the as-deposited films using a 4.1 MeV He beam incident at 10° from the sample normal, with the detector placed at a scattering angle of 170° to optimize the mass resolution of the different elements present. Results have been obtained by simulations with the ion beam analysis software SIMNRA [35], which carries out simulations based on a slab description of the sample. The actual profile likely presents smoother transitions from one material to the next, but this is beyond the resolution of the technique, which is about $1 \times 10^{17} \text{ at. cm}^{-2}$ in this case.

During deposition it was aimed for a thickness of 500 nm, set on a quartz microbalance monitoring system, with some correctable errors in thickness estimation of $\approx 20\%$ due to combined material density and acoustic impedance considerations. The measured thickness is also presented in table 1 (see section 3 for details on the measurements).

3. Spectrophotometry measurements

The dielectric function and the thickness of the coatings were measured by spectrophotometry [36]. Transmission spectra of samples were obtained using an Agilent Cary 5000 spectrophotometer, covering a wide spectral range from 250 nm to 2000 nm, including the absorption onset in the near ultra-violet (UV) region. For coating Run 1, 2 and 4, two samples produced in the same run were measured to check the homogeneity of the coating thickness and eventually the results were averaged. For Run 3, only one sample was available. The measured spectra were analysed using the SCOUT software⁷ in which three different optical models were compared: the Cauchy model [37] in the transparent region in the Visible-Near-Infrared (vis-NIR) range, the Tauc-Lorentz [38] and OJL models [39] in the whole range. While these models are used to investigate different spectral regions, they all cover the NIR region. Therefore, the combined information obtained from the different models allowed us to obtain accurate information on the thickness and refractive index at 1064 nm and 1550 nm of the samples. Coating Runs 1, 2 and 3 have been modelled considering a single thin film on a substrate, while coating Run 4 has been modelled considering the coating structure shown in figure 2, where the total coating is made of three layers of which the middle one is the thickest ($\approx 90\%$ of the total thickness) and consists of almost pure TiO_2 , while the surrounding, thinner layers consist of mixtures of TiO_2 and GeO_2 . Examples of fits to the measured transmission spectra are shown for two examples in figure 2: (A) Coating Run 1 (pure GeO_2 , as deposited) and (B) coating Run 4 (structure of three layers with TiO_2 in the middle, heat treated at 200 °C),

The results obtained for the coating thickness and refractive index at 1064 nm and 1550 nm at room temperature are summarized in tables 1 and 2 respectively, and the refractive indices for different coating runs are shown in figure 2(C). While the refractive indices agree within the error bars, the thickness of samples from the same run shows some variation. Assuming that the thickness variation between samples from the same coating run also indicates a non-uniformity within individual samples, this non-uniformity affects the thickness measurements as follows: the spectrophotometer has a light spot of the order of a few millimetres diameter, covering a relatively large area of the sample and therefore averaging over a potentially non-uniform area, resulting in differences in the fit quality for different samples. For this reasons, we present the average of the results from the same coating run.

While for all coating runs, the refractive indices agree within the error bars at 1064 and 1550 nm, the refractive index is systematically slightly lower at 1550 nm. The refractive index of pure GeO_2 is in agreement with literature values found on similar coatings [40, 41]. The refractive index of the TiO_2 layer in the coating Run 4 structure is 2.2 at 1064 nm. There is a strong variation in literature for n of amorphous TiO_2 thin films, depending on the deposition procedure and conditions. Our result is in agreement with other coatings produced by reactive evaporation ($n = 2.0 - 2.25$, depending on the exact deposition conditions and resulting density [29]). For ion-beam sputtered coatings which are likely more dense, it is usually higher ($n = 2.3$ [27], 2.35 [9], 2.5 [28]).

4. Optical absorption measurements

Spectrophotometry is not suitable for resolving optical absorption at the level present in the films investigated here. Therefore, optical absorption measurements were conducted using photothermal common-path interferometry (PCI) [42]. This method uses a high-intensity

⁷ W. Theiss, Hard-and Software, www.wtheiss.com.

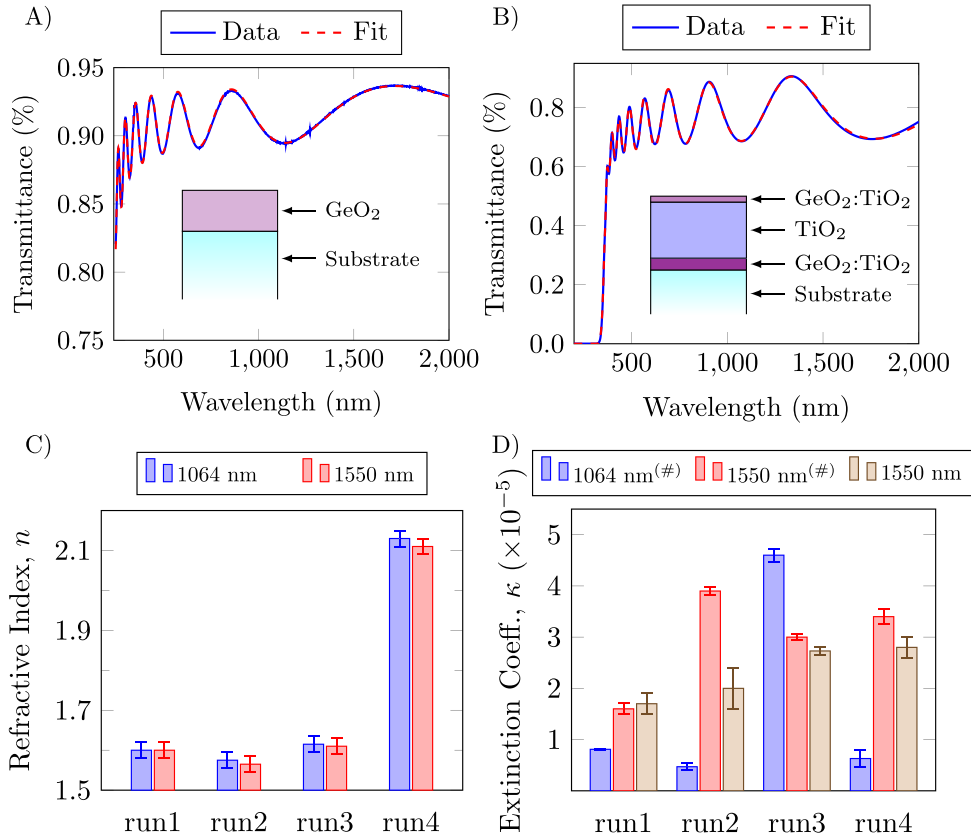


Figure 2. (A) Example of spectrophotometer measurements for Run 1 as deposited. (B) Example of spectrophotometer measurements for Run 4 after annealing at 200 °C. (C) Refractive index at 1064 nm and 1550 nm, for the coatings (as deposited) listed in table 2, obtained by photospectrometry. (D) Extinction coefficient for the coatings (as deposited) listed in table 2 obtained at 1064 nm and 1550 nm, by PCI. Results marked with (#) have been obtained at a different time (approximately 1 year earlier) and in a different PCI setup.

Table 2. Refractive index (n) obtained from spectrophotometry data, and extinction coefficient κ from absorption measurements via PCI, at 1064 nm and 1550 nm for the coatings as deposited. Values highlighted by the symbol (#) have been obtained at a different time (approximately 1 year earlier), in a different PCI setup.

| Run | n @ 1064 nm | n @ 1550 nm | κ @ 1064 nm (#) ($\times 10^{-5}$) | κ @ 1550 nm (#) ($\times 10^{-5}$) | κ @ 1550 nm ($\times 10^{-5}$) |
|-------|-----------------|-----------------|---|---|---|
| Run 1 | 1.60 ± 0.02 | 1.60 ± 0.02 | 0.81 ± 0.04 | 1.60 ± 0.11 | 1.7 ± 0.2 |
| Run 2 | 1.58 ± 0.02 | 1.57 ± 0.02 | 0.47 ± 0.07 | 3.90 ± 0.07 | 2.0 ± 0.4 |
| Run 3 | 1.62 ± 0.02 | 1.61 ± 0.02 | 4.60 ± 0.13 | 3.00 ± 0.06 | 2.73 ± 0.08 |
| Run 4 | 2.22 ± 0.02 | 2.20 ± 0.02 | 0.63 ± 0.16 | 3.40 ± 0.15 | 2.8 ± 0.2 |

‘pump’ laser beam with a waist of approximately $40\ \mu\text{m}$ at the wavelength of interest, i.e. 1064 and 1550 nm. The optical absorption heats the sample in the region hit by the laser beam, resulting in a thermal lens. A second laser beam, which is low in power and approximately three times larger, crosses the pump beam at the sample surface and the inner region of the beam acquires a Gouy phase from the thermal lens. This phase difference relative to the annular outer ring creates an interference pattern along the optical path. By measuring the change in intensity on a photo detector, the absorption of an unknown material can be recovered by comparison to a calibration sample of known absorption. For each sample, the absorption was measured at least in five different regions of the coating and averaged to obtain the results shown. The error bar results from the standard deviation of the results measured in these different regions.

4.1. Absorption of the coatings as deposited at 1550 nm and 1064 nm

The extinction coefficient κ has been obtained from these absorption measurements, together with the thickness and refractive index results presented in the previous section, using the software Tfcalc⁸. Initially, absorption measurements were performed at 1064 and 1550 nm, marked with (#) in table 2 and figure 2. Approximately 1 year later, around the time of the spectrophotometry measurements (and prior to heat treatment—see next section), the measurements were repeated at 1550 nm to check for a possible time evolution of the absorption. For these repeat measurements, a different PCI setup was used. Results for κ for the different coating runs are shown in table 2 and figure 2(D). For coating Run 4, the absorption is entirely attributed to the largest layer of pure TiO_2 and the extinction coefficient values are reported for that layer. This may have led to an over estimation of the absorption of up to 10% in addition to the given error bars.

Although values of κ at 1550 nm measured at different times and in different setups agree within the errors only for Run 1, the values are very close to each other also for the other runs but except Run 2, which may be due to time evolution. However, except for Run 1, the more recently obtained results tend to show lower absorption than the older measurements, which is the opposite from what one would expect: GeO_2 is known to absorb water when stored in air, which would increase the absorption. Another possible explanation for these variations is the non-uniformity of the coating thickness, which translates into an uncertainty in absorption results: as PCI uses a very small laser beam ($\approx 80\ \mu\text{m}$ diameter), the absorption is measured very accurately at a specific point. However, the thickness used to analyse the absorption and calculate κ was obtained by photospectrometry, averaging over a much larger area, and therefore introducing additional uncertainty. This is included in the error bars shown for κ in table 2 obtained from measurements at different positions. Finally, a thickness non-uniformity might be an indicator for variations of other properties, so that any results strongly depend on the region where the absorption is measured.

From looking at the overall trends and not taking off-trend values into account, three main conclusions can be drawn from these results:

- For the coatings investigated here, κ of GeO_2 and TiO_2 is very similar.
- When excluding the unusually high result for Run 2, the level of κ at 1064 nm is in average at around 6×10^{-6} . This is roughly a factor 4 higher than the absorption presented in [28].

⁸ www.spectra.com.

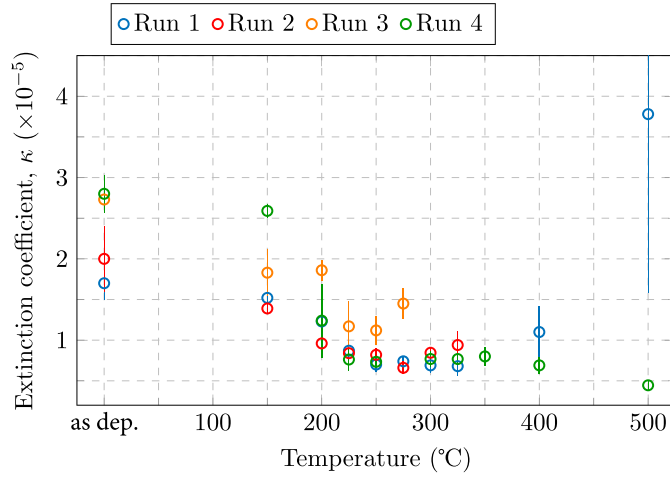


Figure 3. Extinction coefficient measured at 1550 nm as a function of heat treatment temperature for the four coating runs.

However, this absorption value was obtained after heat treatment, while our 1064 nm measurements were obtained before heat treatment. Further improvement with heat treatment can be expected for our coatings (see section 4.2).

- The absorption at 1550 nm is roughly a factor of 5 higher than at 1064 nm. It is unknown if this is intrinsic to the material or due to e.g. impurities.

4.2. Absorption as a function of heat treatment temperature at 1550 nm

In the next step, the samples were heat treated, in air. After initial heat treatments at 150 °C and 200 °C, smaller steps of 25 °C were used to achieve good resolution for the optimum heat treatment temperature at which the absorption minimizes.

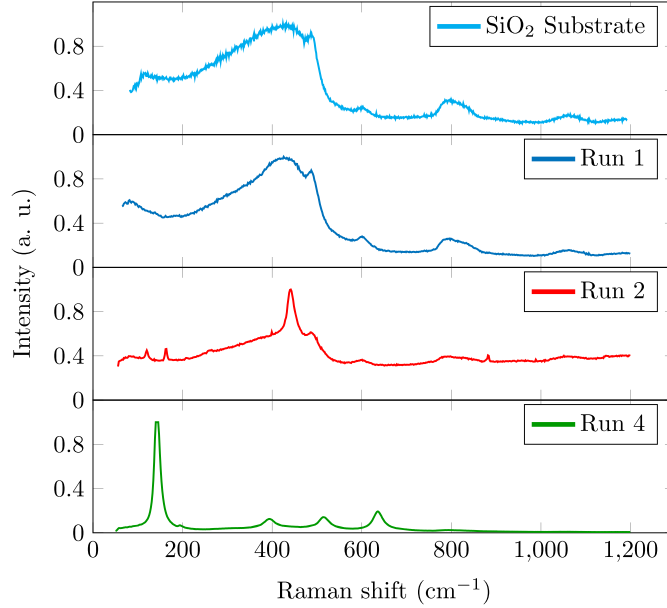
To avoid exceeding the target temperature, a ramp rate of 1 °C min⁻¹ was used during heat up. The samples were held at the target temperature for 4 h. Afterwards they were left to cool down naturally. Following each heat treatment step, the absorption was measured on at least five places across the coating using PCI.

Figure 3 shows the extinction coefficient κ of the coatings at 1550 nm as a function of heat treatment temperature. For all four runs, it can be observed that κ initially decreases. For coating Runs 1, 2 and 3, a minimum forms after which the absorption starts increasing and becomes more scattered across the coating. The minimum of the extinction coefficient for each coating run at the respective heat treatment temperature can be found in table 3. For Run 4, mainly consisting of TiO₂, κ also decreases significantly up to a temperature of ≈ 250 °C. However, other than for the GeO₂ coatings, no clear minimum forms, but κ remains low and homogeneous across the coating. While for Run 1–3, κ reduces by a factor of 2.5 to 3, for Run 4 the lowest absorption is of about 6 \times lower than the as deposited value.

While crystallisation and absorption are not necessarily correlated, an increase in absorption at the onset of crystallisation has been observed for other materials before [9, 43]. Therefore,

Table 3. Temperature and values of the lowest extinction coefficient measured at 1550 nm after annealing for the four coating runs.

| Run | Temperature ($^{\circ}\text{C}$) | κ @ 1550 nm ($\times 10^{-5}$) |
|-------|------------------------------------|---|
| Run 1 | 325 | 0.68 ± 0.12 |
| Run 2 | 275 | 0.66 ± 0.07 |
| Run 3 | 250 | 1.12 ± 0.17 |
| Run 4 | 500 | 0.45 ± 0.06 |

**Figure 4.** Raman measurements of coating Run 1, 2 and 4 after heat treatment at 500°C for Run 1 and 4 and at 325°C for Run 2, and of a SiO_2 substrate for comparison. Each curve has been normalized to be able to observe all the peaks in the same plot. The relevant information for this work are the presence of the peaks to confirm crystallization and the peak positions to define the crystalline phase.

coating Runs 1, 2 and 3 were expected to show an increase in κ at a higher temperature than Run 4 due to the higher crystallisation temperature of GeO_2 compared to TiO_2 .

In order to investigate a possible coating crystallization, Runs 1, 2 and 4 have been analysed using Raman spectroscopy at their final heat treatment temperature. Results are shown in figure 4. The measurements of the sample from Run 1 show a large contribution of the SiO_2 substrate—see SiO_2 spectrum for comparison. This coating is confirmed to still be amorphous after heat treatment at 500°C as no peaks characteristic for crystallisation can be observed. The coating from Run 2 is crystallized as quartz GeO_2 [44], a behaviour possibly related to the small contamination of Ti atoms which might have been sites for crystalline regions. The coating from Run 4 is crystallized as anatase TiO_2 as one would expect [45, 46].

The optimum heat treatment temperature for the coatings from Runs 1–3, which consist of almost pure GeO_2 , is relatively low, and would have been expected to occur at higher

temperatures based on the work by Vajente *et al* [28]. However, the optimum heat treatment temperature for a material depends on the deposition process, and is also affected by degradation of the films during heat treatment and therefore not always intrinsic to the material. For Run 4, on the other hand, it was unexpected that the absorption remained low despite crystallisation, which for TiO₂ usually occurs at around 250 °C–300 °C.

5. Summary

Coatings produced by plasma-assisted ion-beam evaporation in four different runs have been investigated. The composition of the coatings was measured by RBS. While the first three runs showed pure GeO₂ with a small Ti contamination for Run 2 and 3, coating Run 4 showed a layered structure with a pure TiO₂ layer surrounded by thin layers of a mixture of TiO₂ and GeO₂.

The refractive index at 1064 nm and 1550 nm, wavelengths of interest for gravitational-wave detectors, of the pure GeO₂ and pure TiO₂ layers are in agreement with values found in literature.

The optical absorption at both wavelengths for the as deposited coatings was measured in different setups, and at different times, with approximately 1 year between measurements. The most recently obtained results showed lower absorption than the older measurements, in contrast to what is expected due to water absorption of GeO₂ when stored in air. The absorption was found to be similar within all deposition runs (with the exception of a very high value at 1064 nm found for Run 2), indicating similar absorption levels for the GeO₂ and TiO₂ components. The absorption was found to be lower at 1064 nm, where it was in the $\kappa = 10^{-6}$ range for the coatings as deposited, than at 1550 nm, where it was in the 10^{-5} range.

Samples were heat treated in steps and the absorption was measured at 1550 nm, showing a minimum in κ for Runs 1, 2 and 3, at which it decreased by a factor of 2.5–3 compared to that of the as deposited coatings. For Run 4, after initially decreasing, κ formed a ‘low- κ plateau’ with a slightly decreasing trend towards higher heat treatment temperatures. The lowest κ measured was at 4.5×10^{-6} , which is about six times lower than for the coating as deposited. During the analysis, all the absorption was attributed to the TiO₂ layer. This minimum κ corresponds to an absorption of ≈ 10 ppm when used in a highly-reflective coating stack together with SiO₂ as the low-index material. While this is about an order of magnitude higher than required for gravitational-wave detectors, this level is comparable to other coatings in the development phase.

Based on the absorption reduction with heat treatment observed at 1550 nm, the absorption of the coatings at 1064 nm is assumed to be in the low 10^{-6} range after heat treatment, which is comparable to the absorption presented in [28].

Raman studies confirmed that coatings from Run 1 (pure GeO₂) had not crystallized after heat treatment at temperatures at which the absorption starts to increase, while coatings from Run 2 (GeO₂ with small Ti-contamination) showed signs of crystallisation. Run 4 (mainly pure TiO₂), was fully crystallized, which makes the continuous reduction in absorption with heat treatment very interesting, in particular in combination with the previously observed reduction in mechanical loss after crystallisation [33]. Recently, it has also been shown that a mixture of TiO₂ and SiO₂ shows excellent mechanical and optical properties, including low scattering, beyond the crystallisation point [16]. Therefore, further studies of high-quality TiO₂ thin films are of significant interest, even beyond the crystallisation point, for future gravitational-wave detectors.




Data availability statement

The data that support the findings of this study are openly available at the following URL/DOI: <https://doi.org/10.5281/zenodo.10837975> [47].

Acknowledgments

We are grateful for financial support from STFC (ST/V005634/1, ST/V001736/1), the University of Glasgow, the Royal Society (RG110331), ETpathfinder (Interreg Vlaanderen-Nederland), E-TEST (Interreg Euregio Meuse-Rhine), and the Province of Limburg. We thank our colleagues within the LIGO Scientific Collaboration and Virgo Collaboration and within SUPA for their interest in this work. The work done at U. Montréal was supported by the NSERC, and the FRQNT through the RQMP. This publication is part of the project with Project No. VI.Vidi.203.062 financed by the Dutch Research Council (NWO). This article has LIGO Document No. P2300408.

ORCID iDs

A Amato  <https://orcid.org/0000-0001-9557-651X>
V Spagnuolo  <https://orcid.org/0000-0002-0098-4260>
G I McGhee  <https://orcid.org/0000-0001-5038-2658>
M Chicoine  <https://orcid.org/0000-0003-0630-3996>
J Hough  <https://orcid.org/0000-0003-3242-3123>
R Johnston  <https://orcid.org/0000-0002-1312-7268>
R Keil  <https://orcid.org/0009-0009-7527-7040>
S Rowan  <https://orcid.org/0000-0002-0666-9907>
F Schiettekatte  <https://orcid.org/0000-0002-2112-9378>
S C Tait  <https://orcid.org/0000-0003-0327-953X>
I W Martin  <https://orcid.org/0000-0001-7300-9151>
J Steinlechner  <https://orcid.org/0000-0002-6697-9026>

References

- [1] Abbott B P *et al* (The LIGO Scientific Collaboration and Virgo Collaboration) 2016 *Phys. Rev. Lett.* **116** 061102
- [2] Abbott R *et al* (LIGO Scientific Collaboration and Virgo Collaboration) 2021 *Phys. Rev. X* **11** 021053
- [3] Abbott R *et al* 2021 GWTC-3: compact binary coalescences observed by LIGO and Virgo during the second part of the third observing run (arXiv:2111.03606v2)
- [4] The LIGO Scientific Collaboration 2015 *Class. Quantum Grav.* **32** 074001
- [5] Acernese F *et al* 2015 *Class. Quantum Grav.* **32** 024001
- [6] Miller J, Barsotti L, Vitale S, Fritschel P, Evans M and Sigg D 2015 *Phys. Rev. D* **91** 062005
- [7] Harry G M *et al* 2002 *Class. Quantum Grav.* **19** 897
- [8] Hong T, Yang H, Gustafson E K, Adhikari R X and Chen Y 2013 *Phys. Rev. D* **87** 082001
- [9] Granata M *et al* 2020 *Class. Quantum Grav.* **37** 095004
- [10] Larsen B, Ausbeck C, Bennet T F, DeSalvo G, DeSalvo R, LeBohec T, Linker S, Mondin M and Neilson J 2021 *Nanomaterials* **11** 3444
- [11] Amato A *et al* 2021 *Phys. Rev. D* **103** 072001
- [12] Medina J L, Arce J L V, Pizá-Ruiz P, Nedev N R, Farías M H and Tiznado H 2022 *Ceram. Int.* **48** 17564–75

- [13] Pan H W, Kuo L C, Chang L A, Chao S, Martin I W, Steinlechner J and Fletcher M 2018 *Phys. Rev. D* **98** 102001
- [14] Steinlechner J, Krüger C, Martin I W, Bell A, Hough J, Kaufer H, Rowan S, Schnabel R and Steinlechner S 2017 *Phys. Rev. D* **96** 022007
- [15] Granata M et al 2020 *Appl. Opt.* **59** A229–35
- [16] McGhee G I et al 2023 *Phys. Rev. Lett.* **131** 171401
- [17] Amato A, Terreni S, Granata M, Michel C, Sassolas B, Pinard L, Canepa M and Cagnoli G 2020 *Sci. Rep.* **10** 1670
- [18] Yang L et al 2021 *Sci. Adv.* **7** eabh1117
- [19] Bassiri R, Evans K, Borisenko K, Fejer M, Hough J, MacLaren I, Martin I, Route R and Rowan S 2013 *Acta Mater.* **61** 1070–7
- [20] Granata M et al 2018 *Phys. Rev. Mater.* **2** 053607
- [21] Hamdan R, Trinastic J P and Cheng H P 2014 *J. Chem. Phys.* **141** 054501
- [22] Prasai K, Bassiri R, Cheng H P and Fejer M M 2021 *Phys. Status Solidi b* **258** 2000519
- [23] Prasai K et al 2019 *Phys. Rev. Lett.* **123** 045501
- [24] Amato A, Terreni S, Granata M, Michel C, Pinard L, Gemme G, Canepa M and Cagnoli G 2019 *J. Vac. Sci. Technol. B* **37** 062913
- [25] Vajente G et al 2018 *Class. Quantum Grav.* **35** 075001
- [26] Amato A et al 2019 *J. Phys. Mater.* **2** 035004
- [27] Flaminio R, Franc J, Michel C, Morgado N, Pinard L and Sassolas B 2010 *Class. Quantum Grav.* **27** 084030
- [28] Vajente G et al 2021 *Phys. Rev. Lett.* **127** 071101
- [29] Mergel D, Buschendorf D, Eggert S, Grammes R and Samset B 2000 *Thin Solid Films* **371** 218–24
- [30] ET Steering Committee Editorial Team 2020 *Preprint* ET-0007B-20 (available at: <https://apps.et-gw.eu/tds/ql/?c=15418>)
- [31] Adhikari R X et al 2020 *Class. Quantum Grav.* **37** 165003
- [32] Khadka S, Markosyan A, Prasai K, Dana A, Yang L, Tait S C, Martin I W, Menoni C S, Fejer M M and Bassiri R 2023 *Class. Quantum Grav.* **40** 205002
- [33] Robie R 2018 Characterisation of the mechanical properties of thin-film mirror coating materials for use in future interferometric gravitational-wave detectors *PhD Thesis* University of Glasgow (available at: <https://inspirehep.net/literature/1780735>)
- [34] W K Chu, J W Mayer and M A Nicolet (eds) 1978 Copyright *Backscattering Spectrometry* (Academic) (available at: www.researchgate.net/publication/237064389_Backscattering_Spectrometry_Wei-Kan_Chu_James_W_Mayer_and_Marc-A_Nicolet_Academic_Press_1978)
- [35] Mayer M 1999 *AIP Conf. Proc.* **475** 541–4
- [36] Stenzel O and Wilbrandt S 2018 *In Situ and Ex Situ Spectrophotometric Characterization of Single- and Multilayer-Coatings I: Basics* (Springer) pp 177–202
- [37] Stenzel O and Ohlídal M 2018 *Optical Characterization of Thin Solid Films* vol 64 (Springer) (<https://doi.org/10.1007/978-3-319-75325-6>)
- [38] Tauc J 2012 *Amorphous and Liquid Semiconductors* (Springer) (<https://doi.org/10.1007/978-1-4615-8705-7>)
- [39] Musila N, Munji M, Simiyu J, Masika E and Nyenge R 2018 *Path Sci.* **4** 3001–12
- [40] Devyatykh G G et al 1980 *Sov. J. Quantum Electron.* **10** 900
- [41] Hu Y Z, Zettler J, Chongsawangvirod S, Wang Y Q and Irene E A 1992 *Appl. Phys. Lett.* **61** 1098–100
- [42] Alexandrovski A, Fejer M, Markosian A and Route R 2009 Photothermal common-path interferometry (PCI): new developments *Proc. SPIE* **7193** 71930D
- [43] Abernathy M R et al 2011 *Class. Quantum Grav.* **28** 195017
- [44] Madon M, Gillet P, Julien C and Price G D 1991 *Phys. Chem. Miner.* **18** 7–18
- [45] Kernazhitsky L, Shymanovska V, Gavrilko T, Naumov V, Fedorenko L, Kshnyakin V and Baran J 2014 *Ukrainian J. Phys.* **59** 246–53
- [46] Hsu L S and She C Y 1985 *Opt. Lett.* **10** 638–40
- [47] Steinlechner J 2024 Optical properties of germania and titania at 1064nm and at 1550nm *Zenodo* (<https://doi.org/10.5281/zenodo.10837976>)